Tunable optical properties of transition metal dichalcogenide nanoparticles synthesized by femtosecond laser ablation and fragmentation

Anton S Chernikov, Gleb I Tselikov, Mikhail Yu Gubin, Alexander V Shesterikov, Kirill S Khorkov, Alexander V Syuy, Georgy A Ermolaev, Ivan S Kazantsev, Roman I Romanov, Andrey M Markeev, et al.

Journal Name

ARTICLE TYPE

Cite this: DOI: 00.0000/xxxxxxxxxx

Tunable optical properties of transition metal dichalcogenide nanoparticles synthesized by femtosecond laser ablation and fragmentation†

Anton S. Chernikov,[a] Gleb I. Tselikov,[b] Mikhail Yu. Gubin,*[b,a] Alexander V. Shesterikov,[b,a] Kirill S. Khorkov,[a] Alexander V. Syuy,[b] Georgy A. Ermolaev,[b] Ivan S. Kazantsev,[b] Roman I. Romanov,[c] Andrey M. Markeev,[b] Anton A. Popov,[c] Gleb V. Tikhonowski,[c] Olesya O. Kapitanova,[d] Dmitry A. Kochuev,[a] Andrey Yu. Leksin,[a] Daniil I. Tselikov,[c] Aleksey V. Arsenin,[b] Andrei V. Kabashin,[c] Valentyn S. Volkov,[b] and Alexei V. Prokhorov[b,a]

Received Date
Accepted Date

DOI: 00.0000/xxxxxxxxxx

Manipulation of resonant dielectric nanostructures is of paramount importance for next-generation photonic devices. Traditionally, researchers use two-dimensional or phase-change materials for this purpose. However, the former leads to small efficiency, while the latter lacks continuous changes. Here, we provide an alternative approach through laser-induced modification. Specifically, via laser ablation process we synthesized molybdenum disulfide (MoS_2) nanoparticles (NPs), whose composition we then controlled through laser fragmentation. It causes a transformation of MoS_2 into its oxide MoO_{3-x}, which, in turn, results in pronounced modification of optical response, owing to large difference between their optical constants. In addition, laser-fragmented NPs have several times larger photothermal response, compared to original MoS_2 and classical silicon NPs. Thus, our MoS_2-based laser-tunable NPs open up new perspective for resonant nanophotonics, in particular, photothermal therapy.

1 Introduction

The rise of two-dimensional (2D) materials[1] begin a new a technological era in human society. They not only ease the research of fundamental phenomena[2], including quantum Hall effect[3], superconductivity[4], excitons[5–7], trions[8], plasmonics[9], and massless fermions[10], but enable rapid advances in ultrafast photodetectors[11], sensitive biosensors[12,13], room temperature gas sensors[14–16], efficient modulators[17], nanoscale light emitters[18], solar cells[19], on-chip computing[20], and wearable medicine[21]. Besides, their 2D nature results in large optical response, manifesting in high refractive index[6,22], giant optical anisotropy[23], and tightly bound electron-hole pairs[24]. These unique characteristics make van der Waals (vdWs) monolayers an ideal platform for optical applications[25], in particular, to all-dielectric nanophotonics, which utilize the resonant behavior of high-index nanoresonators[26–31]. However, close examination reveals that although monolayers demonstrate record-high efficiency per thickness[32], their device performance is limited by their atomic thickness and requires sophisticated optical design[12,33].

It inspired researchers to shift attention to their bulk counterparts[34] since they preserve advantages of monolayers, namely, large optical constants[6], asymmetrical optical response[23,35], and excitonic dielectric function[36], thanks to weak vdW bonding between layers. As a result, layered materials have already demonstrated great results in subdiffractional guiding[23,37], integrated circuits[38], strong light-matter coupling[39–41], resonance nonlinear processes[28,42], polaritonic transport[23,43], anisotropic metasurfaces[31,44], and photothermal conversion[45], especially, in the case of transition metal dichalcogenides (TMDCs). Besides, recent works[40,45–48] establish fabrication processes of TMDCs nanostructures compatible with widespread complementary metal oxide technologies[49]. In this regard, special attention should be devoted to the laser ablation method for the creation of spherical TMDC nanoparticles[45]. This approach yields mobile spherical nanoresonators, which can be easily incorporated into any optical element, unlike standard lithography processes, used for TMDCs[40,46,47]. Still, the problem of tunable bulk TMDCs nanoresonators remains unsolved because they do not have atomic thickness, which is readily by electrical gating[50] or

[a] Department of Physics and Applied Mathematics, Vladimir State University named after A. G. and N. G. Stoletovs (VlSU), Vladimir 600000, Russia.
[b] Center for Photonics and 2D Materials, Moscow Institute of Physics and Technology (MIPT), Dolgoprudny 141701, Russia. E-mail: myugubin@gmail.com
[c] National Research Nuclear University MEPhI, Moscow 115409, Russia.
[d] Faculty of Chemistry, Lomonosov Moscow State University, Moscow 119991, Russia.
† Electronic Supplementary Information (ESI) available: Additional figures, XPS spectra, and data for atomic concentrations. See DOI: 00.0000/00000000.

by the choice of the substrate[51].

In this study, we propose to manipulate TMDC optical response through laser-induced transformation. More specifically, we adopted laser ablation and fragmentation methods[45,52–58] from MoS_2 targets to synthesize TMDC nanoparticles with varied chemical composition and, hence, modified optical properties within wide range of parameters. Therefore, our work offers an innovative approach to control characteristics of TMDC-based photonic devices and expand the scope of their applications.

2 Experimental setup and measurement techniques

2.1 Synthesis of NPs by *femtosecond laser ablation and fragmentation methods*

We applied a combined method for the synthesis of MoS_2 NPs. At the first step, the laser ablation of rather large NPs in the liquid was used, and, at the second step, laser fragmentation with duration τ_{FR} was utilized for the morphological and chemical transformation of these NPs.

Synthesis of MoS_2 NPs using laser ablation in a liquid followed by particle fragmentation was carried out by means of femtosecond Yb:KGW laser system (Avesta, Russia): the wavelength 1030 nm, maximum pulse energy 150 μJ, pulse duration 280 fs, and pulse repetition rate 10 kHz. The target was a synthetically grown bulk MoS_2 crystal placed in a cuvette filled with 5 ml of liquid. Deionized water (DI water) and ethanol were used as the liquid in which we carry out the laser ablation and further fragmentation. The processing area was a square with a side of 5 mm. Laser beam scanning on the target surface during laser ablation in liquid was carried out using a biaxial deflection system (X-Y galvanometer scan head) RLA-1504 (RAYLASE GmbH, Weßling, Germany): the density of scanning tracks 20 lines/mm and scanning speed 100 mm/s. The laser beam was focused by F-Theta objective with a working distance of 200 mm; the waist diameter of the beam is 50 μm. During laser ablation in a liquid and laser fragmentation of the obtained colloidal solutions, the pulse energy was fixed at 100 μJ (energy flux density 5.095 J/cm^2, pulse repetition rate 10 kHz) and remained unchanged in all experiments. The required pulse energy was reached by using a polarization attenuator, which is a combination of a half-wave plate and a polarization beam splitter.

The process of laser ablation synthesis of MoS_2 NPs in DI water took 5 minutes with a number of passes of 60. To perform the laser fragmentation of MoS_2 NPs, the colloidal solution obtained after the laser ablation was poured into a polystyrene test tube with the magnetic stirring bar at the bottom. A test tube with a colloidal solution was mounted on a magnetic stirrer, which rotated the magnetic stirring bar at 400 rpm and stirred the suspension during the laser treatment. The laser beam was focused into the colloidal solution, while the position of the waist region was set 10 mm below the air/liquid interface. The position of the laser beam did not change over the laser treatment. Laser fragmentation was carried out at room temperature and took from 10 to 60 minutes in increments of 10 minutes. Photographs of the laser ablation process of the MoS_2 crystal and the fragmentation process in DI water are shown in Fig. 1a on left and right, respectively. Several similar colloidal solutions were prepared. Next, the solutions obtained at different durations of the fragmentation process and after the ablation process were studied by different methods: measurement of optical absorption spectra, imaging of particles using TEM, analysis of Raman spectra, determination of hydrodynamic sizes of NPs, analysis of band structure by XPS.

2.2 Investigation of optical properties of obtained NPs solutions by *optical spectroscopy, Raman microscopy/spectroscopy, and spectroscopic ellipsometry*

The optical absorption spectra of the obtained colloidal solutions were measured using a spectrophotometer including monochromator MDR-206 (LOMO Photonics, Saint-Petersburg, Russia) with silicon photodetector, halogen lamp used as a light source, as well as a collimator for obtaining parallel light beams. All measurements were carried out in the wavelength range from 400 to 1100 nm with different time delay $\Delta\tau$ after fragmentation. The hydrodynamic sizes of NPs obtained after laser ablation in a liquid, as well as after laser fragmentation, were determined using particle size analyzer LB-550 (Horiba Ltd., Tokyo, Japan), whose operation principle is based on the dynamic light scattering (DLS). Raman spectra of NPs deposited on the silicon substrate were measured in backscattering geometry using a probe nanolaboratory NTEGRA Spectra (NT-MDT, Zelenograd, Russia), which is the confocal Raman microscopy/spectroscopy integrated with the scanning probe microscope. The diffraction grating with 1800 lines/mm was used for measurements. The diode-pumped solid-state laser (DPSS) generating radiation at the wavelength 473 nm was utilized as an excitation source in the study of all samples.

To study the effective optical constants of synthesized NPs they were deposited as a form of thin films using a vacuum filtration technique[59] on a sapphire membrane with an average hole size of 20 nm. For investigation of effective optical constants of deposited films, we implemented spectroscopic ellipsometry using VASE ellipsometer (J.A. Woollam Co., Lincoln, NE, USA) at multiple incident angles 50°–70° in 5° step and over a broad spectral range from 400 to 1600 nm.

2.3 Characterization of chemical composition of obtained NPs by *scanning transmission electron microscopy and X-ray photoelectron spectroscopy*

The atomic composition of the synthesized NPs was characterized by a scanning transmission electron microscopy (STEM) system (MAIA 3, Tescan, Czech Republic) operating at 0.1–30 kV coupled with an EDS detector (X-act, Oxford Instruments, High Wycombe, UK). Samples for scanning electron microscopy (SEM) imaging were prepared by dropping 2 μL of the NPs solution onto a cleaned silicon substrate with subsequent drying at ambient conditions. Morphological and structural properties of synthesized NPs were characterized by the high-resolution transmission electron microscopy (HR-TEM) system (JEOL JEM 2010) operating at 200 kV with a Gatan Multiscan CCD in imaging and diffraction modes. Samples were prepared by dropping 2 μL of NPs solution onto a carbon-coated TEM copper grid and subsequent

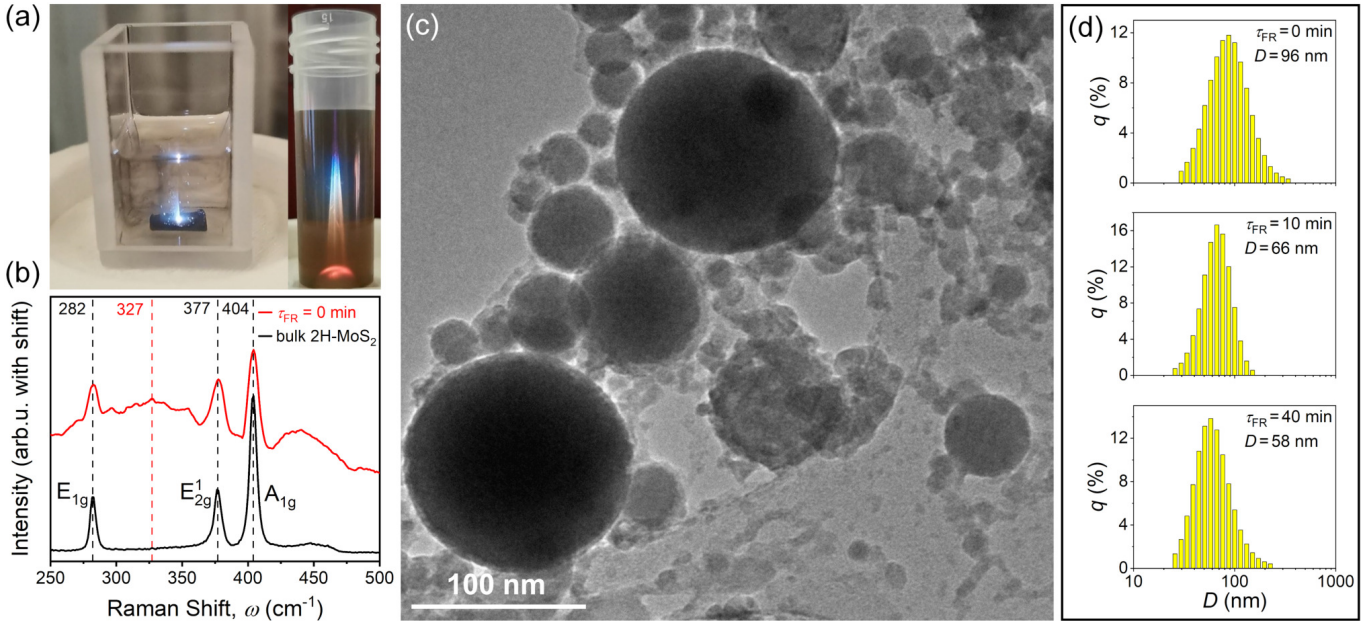

Fig. 1 (a) Photographs of the process of laser ablation of the MoS_2 crystal (left) and the process of laser fragmentation of NPs (right) in DI water. (b) Raman spectra of synthetically grown MoS_2 crystal (black curve) and NPs obtained by laser ablation and deposited on the silicon substrate (red curve). (c) TEM image of NPs obtained after the process of fragmentation during 10 minutes in DI water. (d) Histograms of the distribution of NPs size (q is the percentage of the total number of particles) for the solution after laser ablation, as well as for the solution after laser fragmentation during 10 and 40 minutes (measurements were carried out using the DLS method).

drying at ambient conditions.

Surface composition and the optical band gap value of the synthesized NPs were analyzed by X-ray photoelectron spectroscopy (XPS) using a Theta Probe tool (Thermo Scientific) under high-vacuum conditions using a monochromatic Al-Kα X-ray source (1486.6 eV). XPS spectra were measured using fixed analyzer transmission mode at 50 eV pass energy. The calibration was carried out by the C 1s peak centered at 284.5 eV. The XPS spectra for Mo_{3d}, O_{1s} and S_{2p} were measured along with the spectra of valence bands. The samples were prepared by dropping 1 mL of NPs solution onto a Si substrate with subsequent drying at ambient conditions.

3 Results and discussion

3.1 Laser ablation and fragmentation in deionized water

The initial solutions of MoS_2 NPs were obtained using the laser ablation process in DI water. Its structural composition was confirmed by the analysis of the Raman spectra of the solution and their comparison with the reference curves[60,61] in Fig. 1b. The analysis of the scattering peaks allows us to conclude that the NPs obtained after the process of ablation consist mainly of the 2H-MoS_2 phase. The most probable particle diameter in the solution obtained after the laser ablation was measured using the DLS method and equals to $D = 96$ nm. At the same time, the size of particle lies in the range from 30 to 340 nm, see Fig. 1d. The measured results for zeta potential distribution, shown in Fig. S1 in the Supplementary Information, proves the high stability of the obtained colloids.

Next, the obtained solution was used in the process of laser fragmentation, which led to the formation of MoS_2 NPs with an almost ideal spherical shape. In particular, the TEM image of NPs obtained by laser fragmentation during 10 minutes of the solution after ablation is shown in Fig. 1c. In this case, the laser fragmentation leads to the decrease in the most probable NP size to 66 and 58 nm for 10 and 40 minutes, respectively. At the same time, the range of NP size is also reduced from 25 to 150 nm and from 25 to 225 nm for 10 and 40 minutes, respectively, see Fig. 1d. We also note the presence of peaks corresponding to MoS_2 material in the Raman spectra measured after different fragmentation times. This indicates that MoS_2 phase is retained in the studied NPs.

3.2 Optical properties of NPs obtained in the solution with DI water

Figure 2a shows the optical absorbance spectra of the solution after laser ablation of MoS_2 crystal in DI water, as well as after laser fragmentation during 10 and 40 minutes. First, we note that an increase in fragmentation time leads to a decrease in the absorbance of solutions in the entire spectral range. Such a change in absorbance intensity can be explained by a decrease in the number of highly absorbing NPs that undergo chemical transformations during laser fragmentation. In addition, after the laser treatment, the process of decreasing the absorbance of the solution continues. This indicates that there is a medium initiating further chemical reactions in the solution.

Second, we note a blueshift of the maximum of absorbance curve with increasing fragmentation time. We associate this blueshift with the spectral shift of Mie resonances owing to the decrease in the most probable NP size of highly absorbing high refractive index MoS_2 NPs, see Fig. 1d. Taking into account the

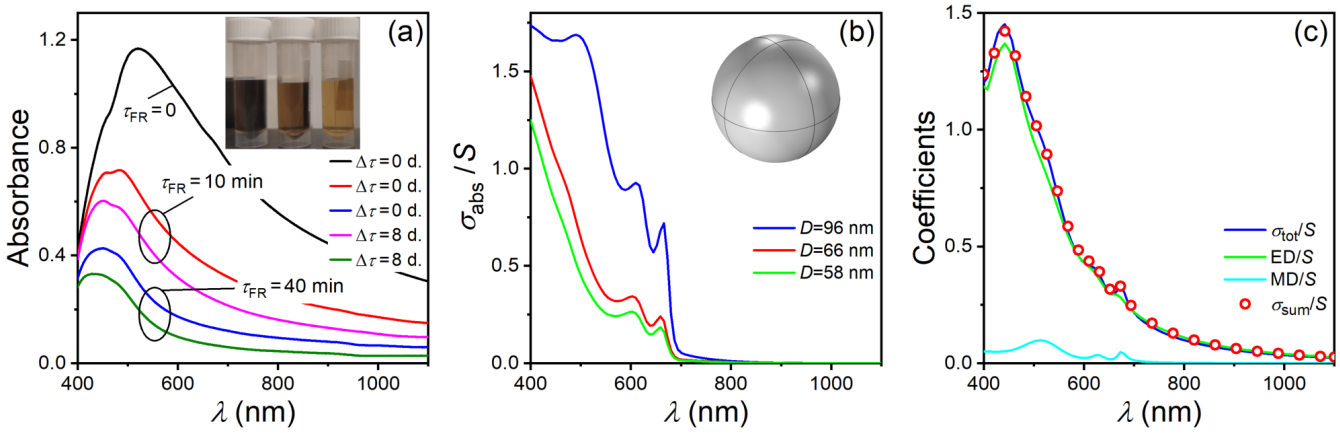

Fig. 2 (a) Optical absorbance spectra for a solution obtained after laser ablation of a MoS_2 crystal in DI water (black curve, corresponds to Fig. 1d for $D = 96$ nm), the solution obtained after laser fragmentation during 10 (pink and red curves, correspond to Fig. 1d for $D = 66$ nm), and 40 (green and blue curves, correspond to Fig. 1d for $D = 58$ nm) minutes. The absorbance curves measured for the solutions at the day of preparation and 8 days after preparation upon keeping the solutions at a temperature of 6°C are indicated by ovals. The inset: solutions obtained after (from left to right) laser ablation and subsequent fragmentation during 10 and 40 minutes. (b) Absorption cross sections and (c) scattering cross section and contributions of the dipole moments for NP with $D = 96$ nm calculated using the permittivity (4) and formulas (1) for spherical NP placed in water and normalized to the geometric cross-section of NP $S = \pi D^2/4$.

relationship between absorption and scattering processes for Mie resonances, the change in the size of scattering NPs can even be detected visually by the color changes of the solutions in test tubes, see the inset in Fig. 2a.

To analyze the spectral dependence of the absorption/scattering cross-section of the considered NPs, we took into account only the dipole response of the NPs assuming that the summed scattering cross-section σ_{sum} of NP irradiated by the plane electromagnetic wave can be represented as $\sigma_{\text{sum}} \cong \text{ED} + \text{MD}$. The contributions of the corresponding dipole terms can be represented through the components of the electric p_i and magnetic m_i dipoles in the following form[62,63]:

$$\text{ED} = \sum_i \text{ED}_i = \frac{k_0^4}{6\pi\varepsilon_0^2 |E_0|^2} \sum_i |p_i|^2, \tag{1a}$$

$$\text{MD} = \sum_i \text{MD}_i = \frac{k_0^4 \varepsilon_d \mu_0}{6\pi\varepsilon_0 |E_0|^2} \sum_i |m_i|^2, \tag{1b}$$

where $i = x, y, z$; ε_d is the relative permittivity of the surrounding medium, E_0 is the electric field of the incident wave at the dipole localization point, k_0 is the wave number in a vacuum, μ_0 is the vacuum permeability, ε_0 is the electric constant. The corresponding components of the dipole moments take the form[63]:

$$\mathbf{p} = \int_V \frac{\mathbf{J}(\mathbf{r})\, j_0(k\mathbf{r})}{-i\omega} d\mathbf{r} - \frac{k^2}{10i\omega} \int_V \frac{15 j_2(k\mathbf{r})}{(k\mathbf{r})^2} \left([\mathbf{r}\cdot\mathbf{J}(\mathbf{r})]\,\mathbf{r} - \frac{1}{3}\mathbf{r}^2 \mathbf{J}(\mathbf{r}) \right) d\mathbf{r}, \tag{2a}$$

$$\mathbf{m} = \frac{3}{2} \int_V \frac{[\mathbf{r}\times\mathbf{J}(\mathbf{r})]\cdot j_1(k\mathbf{r})}{k\mathbf{r}} d\mathbf{r}, \tag{2b}$$

where V is the volume of the scatterer, $\mathbf{r}$ is the radius vector of the unit volume inside the scatterer, $j_j(\rho) = \sqrt{\frac{\pi}{2\rho}} J_{j+1/2}(\rho)$ is the spherical Bessel function of i-th order, k is the wave number in the surrounding medium. The components of the displacement current tensor in (2) have the form:

$$\mathbf{J}(\mathbf{r}) = -i\omega\mathbf{P}(\mathbf{r}) = -i\omega\varepsilon_0 (\varepsilon_p - \varepsilon_d)\,\mathbf{E}(\mathbf{r}), \tag{3}$$

where ω is the angular frequency of the incident field, $\mathbf{P}(\mathbf{r})$ is the polarization vector of the unit volume, ε_p is the relative permittivity of the scatterer, $\mathbf{E}(\mathbf{r})$ is the total electric field inside the particle.

We fulfilled the numerical calculation of the absorption/scattering cross section for the single MoS_2 NP possessing the most probable size obtained experimentally, see Fig. 1d. To calculate the absorption/scattering cross sections, we assume that NP has a spherical shape. The isotropic MoS_2 material (with a disordered arrangement of MoS_2 layers) was considered as the material of NP with the permittivity described as follows

$$\varepsilon_{\text{iso}} = \frac{2}{3}\varepsilon_{\parallel} + \frac{1}{3}\varepsilon_{\perp}, \tag{4}$$

where $\varepsilon_{\parallel}(\varepsilon_{\perp})$ corresponds to the permittivity along(perpendicular to) the layers of the anisotropic MoS_2 material. The data for $\varepsilon_{\parallel}(\varepsilon_{\perp})$ was taken from the Refs. 23,31. We assume that the main contribution to absorption results from NPs with the most probable size, as well as that NPs immersed in solution do not interact with each other, i.e., the effects corresponding to single NP are enhanced in the ensemble due to a large number of the particles. The numerical simulation was carried out using COMSOL Multiphysics.

Figure 2b shows the spectral dependencies of the normalized absorption cross-section σ_{abs}/S, where $S = \pi D^2/4$, for MoS_2 NP with different diameters placed in water. It can be seen that the NP with diameter $D = 96$ nm possesses a double absorption peak in the wavelength range 400–520 nm, which is in qualitative agreement with the experimental curve for the colloidal solution of NPs obtained by laser ablation, see the black curve in

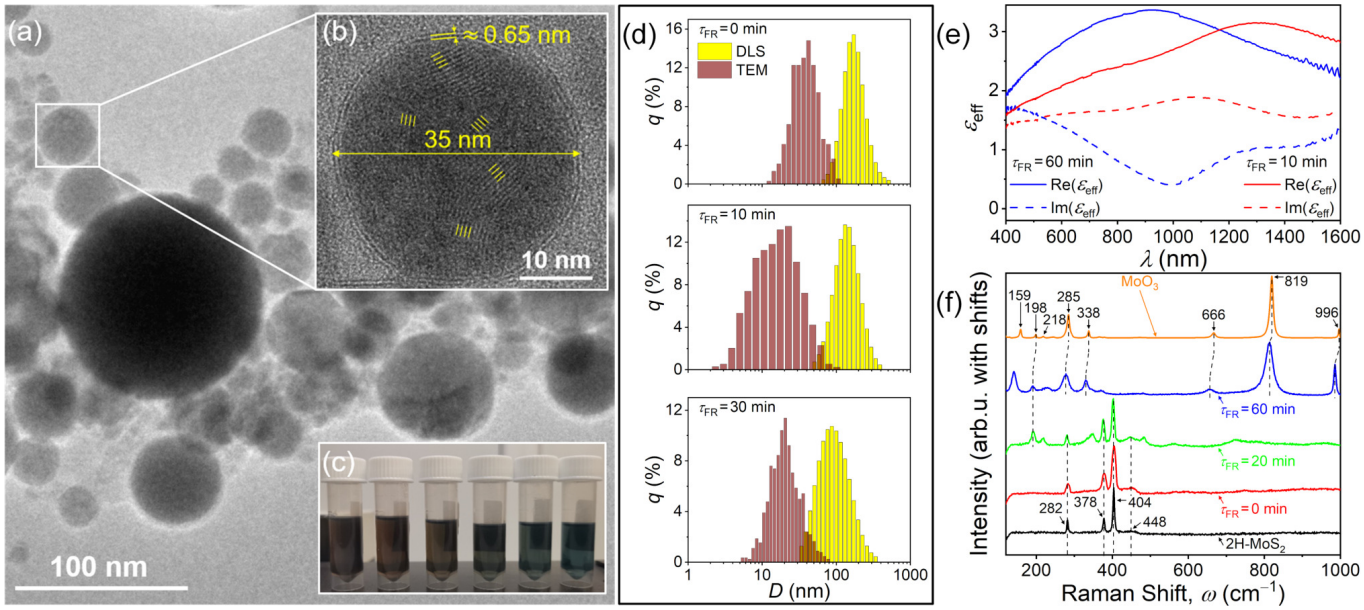

Fig. 3 (a) TEM image of NPs synthesized in ethanol and (b) HR-TEM image of NPs obtained after the process of fragmentation for 10 minutes. (c) Photographs of colloidal solutions obtained after laser fragmentation during (from left to right) 10, 20, 30, 40, 50 and 60 minutes. (d) Histograms of the NPs size distribution for the solutions obtained after laser ablation and laser fragmentation during 10 and 30 minutes were measured by DLS (yellow bars) and TEM (dark red bars) methods. (e) Frequency dependencies for the real Re(ε_{eff}) (blue and green curves) and imaginary Im(ε_{eff}) (red and cyan curves) parts of the effective permittivity of a film made of the solution of NPs, which is obtained by laser fragmentation during 10 (dashed curves) and 60 (solid curves) minutes. (f) Raman spectra of the MoS_2 crystal (black curve) and NPs resulted from the laser ablation (red curve) and subsequent fragmentation for 20 (green curve) and 60 (blue curve) minutes, as well as for MoO_3 material (orange curve) taken from the RRUFF database (ID R210024).

Fig. 2a. The decrease in the NP diameter leads to a blueshift of the absorption peak and decrease in its intensity, see the curves for $D = 66$ nm and $D = 58$ nm in Fig. 2b. This behavior is also in agreement with the experimentally measured dependencies for particles obtained by laser fragmentation during 10 and 40 minutes in Fig. 2a.

Of course, it is difficult to directly compare the obtained numerical and experimental results since NPs in the colloidal solutions have a large size dispersion, see Fig. 1d. Besides, the main mechanism for the analysis of NP size in the DLS method is the light scattering. Therefore, the method errors may occur in the spectral region of Mie resonances for NP due to a significant increase in light scattering.

In particular, Figure 2c shows the spectral dependencies of the scattering cross-sections for MoS_2 NPs with a diameter $D = 96$ nm normalized to the cross-sectional area S of NP, as well as the normalized contributions of electric ED/S and magnetic MD/S dipoles in summed scattering cross-section σ_{sum}. It is clearly seen that the peak of light scattering corresponds to the spectral region of strong absorption for the black curve obtained experimentally in Fig. 2a. We also found that the main scattering mechanism is an electric dipole excited in the NP, see Fig. 2c.

Finally, we should note the almost complete absence of the exciton peaks for the experimental curves in Fig. 2a. Thus, the main mechanism explaining the behavior of the spectral dependencies in Fig. 2a can be the excitation of Mie resonances of high refractive index MoS_2 NPs. At the same time, there is a question: what chemical transformations can occur with NPs leading to a decrease in the absorbance of the solution over time, see Fig. 2a?

3.3 Laser ablation and fragmentation in ethanol

Laser ablation of MoS_2 crystal in ethanol and subsequent fragmentation of the obtained solution also leads to the formation of spherical NPs. Figures 3a and 3b show TEM images of NPs obtained by laser fragmentation during 10 minutes of the solution after ablation. The study of HR-TEM images revealed the core-shell structure of produced NPs. The NP core consists of disordered layers of crystallites and NP shell consists of concentric material layers, see Fig. 3b. The number of shell layers mainly varies from 2 to 3, and the thickness of the material layers for both the core and shell is about of 0.65 nm, see Fig. 3b, which approximately coincides with the thickness of the 2H-MoS_2 layer[64,65]. Analysis of TEM images showed that such NPs are mainly formed after the laser ablation and fragmentation during 10 minutes in ethanol. Such a shell disappears for NPs obtained by fragmentation during or longer than 30 minutes.

Histograms of the size distribution of NPs synthesized in the solutions after laser ablation and fragmentation during 10 and 30 minutes were measured using the DLS method and obtained by the analysis of TEM images. Figure 3d shows a comparison of the results measured by these methods. At the same time, the DLS method gives significantly larger values of the most probable NP size, relative to those obtained by the analysis of TEM images, see Fig. 3d. In particular, the analysis of TEM images results in the most probable NP size of about 36 nm for the solution after laser ablation and approximately the most probable NP size for

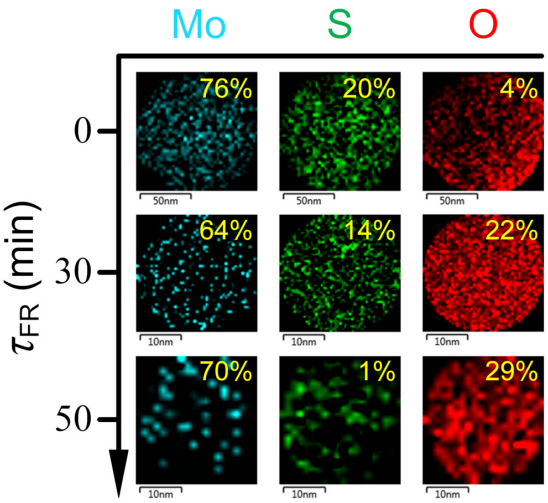

Fig. 4 Spatio-temporal map of the distribution of chemical substances for the single NP from a solution visualized by EDX spectroscopy after keeping the solutions of NPs in ethanol for 30 days at a temperature of 6°C. The analysis was carried out for the most common NPs (with sizes close to the average NP sizes, see Fig. 3d) in solutions after ablation and fragmentation of various durations.

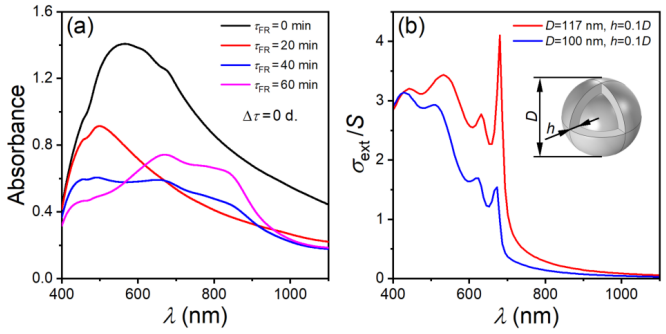

Fig. 5 (a) Optical absorbance spectra for the solutions obtained by laser ablation (black curve), laser fragmentation during 20 (red curve, the most probable NP size $D = 117$ nm), 40 (blue curve, the most probable NP size $D = 100$ nm), and 60 (magenta curve) minutes. (b) Spectral dependences for the extinction cross-section of single core-shell MoS_2 NP placed in ethanol were numerically calculated using the model (4)–(5) for permittivity and normalized to the geometric cross-section of NP $S = \pi D^2/4$. The inset: schematic illustration of core-shell NP with diameter D and shell thickness h.

all solutions after laser fragmentation that equals to 18 nm. At the same time, the DLS method determines the following most probable sizes of NPs: 370 nm, 148 nm and 103 nm for the solutions obtained after laser ablation and fragmentation during 10 and 30 minutes, respectively. We again associate this with the peculiarities of the DLS method, which mainly detects the strongly scattering NPs. As in the case of fragmentation in water, the DLS method detects large MoS_2 NPs, in which strong Mie resonances are excited. However, their number decreases in the process of fragmentation, which is clearly demonstrated by the DLS distributions: an increase in the fragmentation time leads to a decrease in the right tail of the distribution function corresponding to the range of about 100 nm and more. At the same time, we are interested in determining the chemical composition of small NPs with a size of about 18 nm synthesized by fragmentation.

A comprehensive analysis of the chemical composition of colloidal solutions of the obtained NPs was carried out using Raman spectroscopy and energy-dispersive X-ray (EDX) spectroscopy. The comparison of the obtained Raman spectra in Fig. 3f shows that 2H-MoS_2 material is dominated in the solution after laser ablation in ethanol. On the contrary, there are no peaks associated with the 2H-MoS_2 material for the solution of NPs obtained after fragmentation for 60 minutes. However, the Raman spectrum for this solution is well agreed with the spectrum for the MoO_3 material taken from the RRUFF database (ID R210024). A slight shift of the scattering peaks relative to the MoO_3 spectrum is probably due to the thermal effects. At the same time, the Raman spectrum for the solution of NPs obtained after fragmentation during 20 minutes comprises the peaks corresponding to both 2H-MoS_2 and MoO_3 material, see the green curve in Fig. 3f. Thus, the increase in the fragmentation time leads to the transformation of MoS_2 NPs into MoO_3 NPs through the intermediate phase formed in the range of fragmentation duration 20–60 minutes.

Such a transformation is confirmed by the results of the EDX spectroscopy in Fig. 4, where the map of the distribution of chemical elements in the most common NPs in a solution obtained after ablation and different fragmentation times is presented. We note that an increase in the fragmentation time leads not only to the decrease in NP size but also to the development of laser-induced chemical reaction of partially substitution of sulfur atoms for oxygen ones. At the same time, the final product after fragmentation times of 50 minutes or more, indeed, are small MoO_3 NPs. We also suppose that the intermediate product corresponding to the fragmentation time of about 30 minutes is the small NPs of MoO_{3-x}[57,58,66–68], see Fig. 4. Note that the considered processes of substitution of chemical elements in NPs became possible due to the increase in the level of free oxygen in the solution. We suppose that its appearance is associated with the laser-induced decomposition reactions of ethanol molecules. In general, the presented phase transformations should strongly affect the optical spectra of solutions, since the optical characteristics of the initial material MoS_2, intermediate phase MoO_{3-x}, and final material MoO_3 are very different.

The optical characterization of the synthesized NPs was carried out by measuring the absorption spectra for the obtained colloidal solutions of NPs. The measured spectra were compared with the results of the numerical calculation of the extinction cross-section σ_{ext} for single MoS_2 NP by analogous with a water solution. We used the model of spherical core-shell NP with diameter D and shell thickness h in numerical simulation, see the inset in Fig. 5b. We consider that core consists of the isotropic MoS_2 material, as well as for the case of deionized water, with the permittivity described by formula (4), i.e., $\varepsilon_{core} = \varepsilon_{iso}$. At the same time, the anisotropic MoS_2 material with a concentric arrangement of layers was used as the shell material (see Fig. 3b). In this case, the permittivity of NP shell is described as follows:

$$\varepsilon_{shell} = \begin{cases} \varepsilon_{\parallel} & \text{if } \mathbf{E}(\mathbf{r}_s) \perp \mathbf{r}_s \\ \varepsilon_{\perp} & \text{if } \mathbf{E}(\mathbf{r}_s) \parallel \mathbf{r}_s \end{cases}, \quad (5)$$

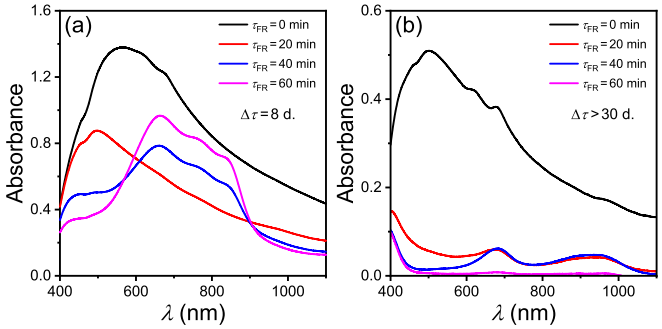

Fig. 6 Optical absorbance spectra for the solutions obtained by laser ablation (black curve), and laser fragmentation during 20 (red curve), 40 (blue curve), and 60 (magenta curve) minutes measured (a) 8 days after preparation, as well as (b) after degradation of the solutions of NPs.

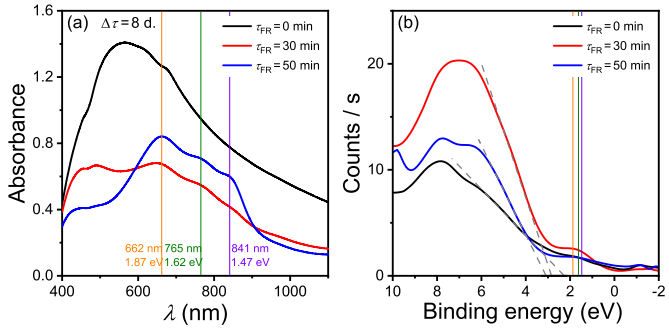

Fig. 7 (a) Comparison of the optical characteristics of the synthesized NPs with the results of XPS measurements. (a) Optical absorbance spectra for the solution obtained by laser ablation of a MoS_2 crystal (black curve) and subsequent laser fragmentation during 30 (red curve) and 50 (blue curve) minutes in ethanol, which were measured 8 days after preparation upon keeping the solutions at a temperature of 6°C. (b) XPS valence-band spectra for the colloidal solution obtained after laser ablation (black curve) and laser fragmentation during 30 (red curve) and 50 (blue curve) minutes in ethanol measured 8 days after preparation upon keeping the solutions at a temperature of 6°C.

where $\mathbf{E}(\mathbf{r}_s)$ is the electric field vector, $\mathbf{r}_s$ is the radius vector of the point inside the shell relative to the center of the spherical NP.

Figures 5 and 6 show the optical absorbance spectra of the solutions obtained after laser ablation of MoS_2 and fragmentation during 20, 40, and 60 minutes in ethanol. The spectra were measured at the day of preparation of the solutions (Fig. 5a) and 8 days after preparation (Fig. 6a) upon keeping the solutions at the temperature of 6°C. Additionally, we measured the absorbance spectra for completely transparent solutions, which were kept at room temperature for a long time. At the same time, one can see in Fig. 5a the tendencies similar to the ablation in water: the blueshift of Mie-induced resonance with increasing fragmentation time and corresponding decrease in NP size. This is confirmed by the results of numerical simulation carried out for core-shell MoS_2 NPs, see Fig. 5b. Note that for the fragmentation times more than 40 minutes, the peak associated with the Mie resonances for MoS_2 NPs almost disappears, see Figs. 5a and 6. Under these conditions, all initial MoS_2 NPs are oxidized and their Mie resonances are shifted beyond the studied spectral range.

However, a decrease in absorbance with increasing fragmentation time is observed only in the spectral range of 450–600 nm, while additional strong absorbance peaks appear in the range of 600–900 nm. At the same time, the color of the solutions changes from dark brown to blue with the increase in the fragmentation time, see Fig. 3c. Note that the detected absorbance peaks became more pronounced 8 days after the preparation of the solutions kept at the temperature of 6°C, see Fig. 6a.

To find out the origin of the absorption peaks, additional studies were fulfilled. In particular, thin films were fabricated by vacuum filtration method from the solutions obtained by laser fragmentation during 10 and 60 minutes, and their ellipsometry was carried out, see Fig. 3e. Based on the spectral dependencies measured for the effective permittivity of the films, one can see that its real part is always positive in the studied spectral range. Thus, we can conclude that the occurrence of the triple peak in Figs. 5a and 6a is not associated with the plasmonic effects.

Next, to assess the chemical composition of samples, we performed XPS measurements (Fig. S1). A detailed study was fulfilled in spectral ranges corresponding to bonds formed by Mo, S and O atoms. No impurities were found during XPS measurements. The Mo3d spectrum was decomposed into several doublets corresponding to Mo^{4+} state in MoS_2 compound and Mo^{6+} state in MoO_3 compound. In addition, the Mo^{5+} state was also registered, it can be assigned to MoS_x or MoSO composition. Also, the peak at 226 eV corresponding to S2s line was presented in the spectrum. The S2p spectra were described by two peaks corresponding to sulfur states in MoS_x and MoSO compounds (163.5 eV) and $(SO_4)^{2-}$ complex (169 eV). The calculated atomic concentration of Mo and S atoms being in different oxidation states can be found in Table S1. It is seen that the relative concentrations of MoS_2, MoS_x, and MoO_3 compounds in the samples change nonmonotonically with time of fragmentation. In particular, NPs synthesized in the solution after laser ablation consists mainly of MoS_2 material with the band gap 2.3 eV[69]. The optical band gap was estimated by extrapolation of the linear portion of the curves in Fig. 7b, i.e., the binding energy in intersection points of linear extrapolations with the zero value of the Counts axis. After the fragmentation process for 50 minutes, the band gap of the studied material changes to 3.2 eV which corresponds to the band gap of MoO_3 [70]. However, this value is outside of the considered spectral range in Fig. 7a, so it does not affect the corresponding absorbance curve in Fig. 7a. At the same time, for the solution of NPs obtained after 30 minutes of fragmentation process, the band gap is already 2.8 eV. In general, the measured value of the band gap corresponds to the suboxide MoO_{3-x} [67]. Besides, the additional peaks appear in the range of 1.4–1.9 eV on the XPS curve in Fig. 7b. We associate them with the appearance of defect levels in the band gap of MoO_{3-x} [58,66], which are actively and firstly populated under the irradiation of the solution. We assume that exactly these features correspond to the appearance of absorbance peaks at 662 nm, 765 nm, and 841 nm for the corresponding curves in Figs. 5a, 6a and 7a. The peculiarity of the observed peaks is that the spectral positions of their maxima are almost independent of the fragmentation time. At the same time, the intensity of the peaks significantly depends on the time

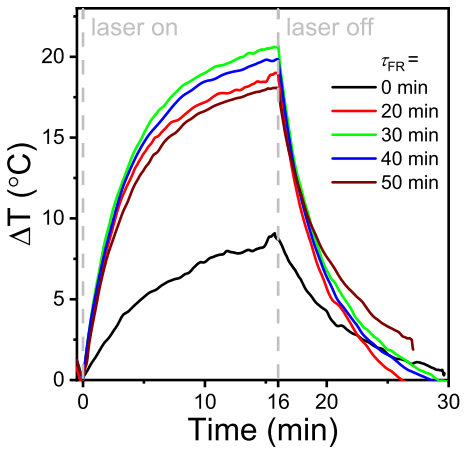

Fig. 8 Temporary dependence of temperature for colloidal MoS_2, MoO_{3-x} and MoO_3 NP solutions during constant photothermal excitation with a power of $P = 0.9$ W at excitation wavelength $\lambda_{exc} = 830$ nm.

of fragmentation/keeping of the solution. Thus, based on the spatio-temporal map in Fig. 4 and band gap variation of NPs in Fig. 7b, it is possible to evaluate the entire process of transformation of the initial MoS_2 material through the intermediate phase MoO_{3-x} into the final MoO_3 material. Of course, to reveal all details of such transformations, the morphology/structure variation of MoS_2, MoO_{3-x}, and MoO_3 compositions should be monitored during the whole process of fragmentation. In particular, it is convenient to determine various compositions by retrieving the lattice spacing using TEM images. Unfortunately, despite the high resolution of the method, this is not always possible. The TEM method allows us to clearly determine the internal structure of only the skin layer at the edge of large NPs when the electron beam passes through the NP along a short chord. One such successful image for NP, where both MoS_2 and MoO_{3-x} lattices exist, is shown in Fig. S2.

We note that regardless of the fragmentation time, all solutions of NPs experience a decrease in the absorbance for the entire spectral range in Fig. 6b. This is apparently caused by the influence of the medium in the solution even in the absence of laser treatment after the fragmentation. The presence of such an environment leads to the gradual transformation of the whole MoS_2 material into MoO_3 oxide. In this case, regardless of the solvent and fragmentation time, the obtained solutions of NPs become transparent over time with the complete transformation of the NPs material into MoO_3 oxide. At the same time, the low refractive index dielectric MoO_3 NPs do not possess the exciton resonances and considerable Mie resonances in the considered spectral range. Remarkably, the solution synthesized by ablation does not become transparent without fragmentation, i.e., the reaction medium is not formed there.

In general, based on the performed studies, the strategy for control and tuning of the optical absorption spectrum of synthesized NPs can be proposed. At the first step, it consists in adjusting the parameters of laser ablation in order to fabricate MoS_2 NPs with the required size. At the same time, it is important to choose the necessary solvent, in particular, ethanol, to enrich the solution with oxygen during the subsequent fragmentation process. Next, at the second step, it is required to precisely control the fragmentation time for the solution after ablation in order to fix the desired proportion of oxygen during the formation of MoO_{3-x} NPs in the solution. This is necessary to tune the absorption spectrum of the solution in the visible range. However, the transformation of MoO_{3-x} up to MoO_3 inside NPs in solution over time is a separate problem that requires the development of methods for the conservation of the obtained NPs for their further use in applications.

We assessed photo heating properties of laser produced colloids in the near-infrared-I (NIR-I) range by controlling the temperature evolution of colloids under continuous wave illumination of laser diode at the wavelength of 830 nm with a power of $P = 0.9$ W and the beam size of 3 mm until thermodynamic equilibrium was reached (~16 minutes). The photothermal responses of laser ablated MoS_2 and laser fragmented MoO_{3-x} and MoO_3 NPs were compared with each other in order to estimate their suitability for theranostics[71,72], see Fig. 8. We conclude that, for the characteristic fragmentation times $\tau_{FR} = 20 - 30$ minutes, the photothermal response of the solution significantly increases (by 2.8 times), which is associated with the formation of MoO_{3-x} NPs and excitation of exciton resonances in them, see Fig. 6a. A further increase in fragmentation time leads to a slight decrease in the photothermal response. We explain this by the fact that photo heating properties were measured after keeping the solutions for 2 months at a temperature of 6°C, which resulted in their partial transparency. In other words, during the keeping of solutions for this period, the MoO_{3-x} NPs experienced partial transformation into MoO_3 NPs, which do not exhibit the exciton resonances near 800 nm, see Fig. 6b. As a result, the obtained MoO_{3-x} NPs demonstrate more bright photothermal properties compared to MoS_2 NPs whose similar properties are 2 times greater than for Si NPs conventionally used in theranostics[45].

Thus, theranostics can become an important practical application of the resulting NPs, taking into account their record heat-conducting properties. On the other hand, laser-synthesized nanoparticles with new optical properties can be the basis for the fabrication of electro-optical devices[68], as well as subdiffraction lattices by laser transfer techniques[73]. Such lattices can be used as optical metasurfaces to control the amplitude-phase[31] and polarization characteristics of light[30], as well as for control of quasi-trapped modes[74].

4 Conclusion

We carried out a comprehensive physicochemical analysis of the synthesized solutions and concluded that fragmentation in water leads to the synthesis of MoS_2 NPs possessing optical properties well described by the Mie theory of light. Fragmentation in ethanol during a time that is greater than the critical one initiates the development of chemical reactions with the formation of an intermediate phase, namely, NPs consisting of MoO_{3-x} suboxides, which exhibit bright exciton resonances. We also note that the reaction medium formed in the solution maintains the process of transformation of MoS_2 into suboxides even after laser irradiation. This leads to the complete transparency of the solu-

tion with the formation of MoO_3 NPs without any considerable optical resonances. Thus, we revealed and visualized the chain of morphological and chemical transformations during femtosecond laser fragmentation of 2D MoS_2 material in various solvents. The obtained MoO_{3-x} NPs in ethanol demonstrated a record value of photothermal response resulted from both the exhibition of the high-refractive-index properties of the initial MoS_2 material and the excitation of bright exciton resonances in suboxide NPs.

The obtained NPs of 2D materials can be used as nano-catalysts of chemical reactions, in medical diagnostics, and for the creation of optical coatings. The greatest potential of the obtained core-shell NPs can be associated with their use as bright chromophores and the creation of lasing devices based on them. At the same time, the issues of obtaining narrowly dispersed NPs of 2D materials, control of the core and shell sizes, and conservation of their chemical composition require additional studies.

Author Contributions

The manuscript was written through the contribution from all authors. Investigation, A.S.C., G.I.T., K.S.K., A.V.S., G.A.E., I.S.K., R.I.R., A.M.M., A.A.P., G.V.T., O.O.K., D.A.K., D.I.T.; validation, A.S.C., G.I.T., K.S.K., A.V.S., G.A.E., I.S.K., R.I.R., A.M.M., A.A.P., G.V.T., D.I.T.; methodology, A.S.C., G.I.T., M.Yu.G., K.S.K., A.V.S., G.A.E., O.O.K., D.A.K., A.V.P.; visualization, A.S.C., M.Yu.G., O.O.K.; writing-original-draft, A.S.C., G.I.T., M.Yu.G., G.A.E., A.V.P.; resources, G.I.T., K.S.K., A.V.S., G.A.E., D.A.K.; formal-analysis, M.Yu.G., A.V.S., O.O.K., A.V.P.; writing-review-editing, M.Yu.G., A.V.P.; software, A.V.S., A.Yu.L.; funding-acquisition, A.V.A., V.S.V., A.V.P.; supervision, conceptualization, and project-administration, A.V.A., A.V.K., V.S.V., A.V.P.

Conflicts of interest

There are no conflicts to declare.

Acknowledgements

Authors thank Prof. A.B. Evlyukhin for helpful discussions and Prof. T.A. Trifonova for help in experiments on dynamic light scattering. This work was supported by the Ministry of Science and Higher Education of the Russian Federation (Agreement No. 075-15-2022-1150). Fabrication and chemical characterization of samples were supported by the Russian Science Foundation (Grant No. 21-79-00206). Development of numerical algorithms and optical characterization of the solutions were supported by the Ministry of Science and Higher Education of the Russian Federation (Grant No. FZUN-2020-0013).

Notes and references

1 K. S. Novoselov, A. K. Geim, S. V. Morozov, D. Jiang, Y. Zhang, S. V. Dubonos, I. V. Grigorieva and A. A. Firsov, *Science*, 2004, **306**, 666–669.

2 K. I. Bolotin, F. Ghahari, M. D. Shulman, H. L. Stormer and P. Kim, *Nature*, 2009, **462**, 196–199.

3 K. S. Novoselov, Z. Jiang, Y. Zhang, S. V. Morozov, H. L. Stormer, U. Zeitler, J. C. Maan, G. S. Boebinger, P. Kim and A. K. Geim, *Science*, 2007, **315**, 1379.

4 J. M. Park, Y. Cao, L.-Q. Xia, S. Sun, K. Watanabe, T. Taniguchi and P. Jarillo-Herrero, *Nat. Mater.*, 2022, **21**, 877–883.

5 G. Wang, A. Chernikov, M. M. Glazov, T. F. Heinz, X. Marie, T. Amand and B. Urbaszek, *Rev. Mod. Phys.*, 2018, **90**, 021001.

6 G. A. Ermolaev, Y. V. Stebunov, A. A. Vyshnevyy, D. E. Tatarkin, D. I. Yakubovsky, S. M. Novikov, D. G. Baranov, T. Shegai, A. Y. Nikitin, A. V. Arsenin and V. S. Volkov, *npj 2D Mater. Appl.*, 2020, **4**, 21.

7 C. Trovatello, F. Katsch, N. J. Borys, M. Selig, K. Yao, R. Borrego-Varillas, F. Scotognella, I. Kriegel, A. Yan, A. Zettl, P. J. Schuck, A. Knorr, G. Cerullo and S. Dal Conte, *Nat. Commun.*, 2020, **11**, 5277.

8 K. F. Mak, K. He, C. Lee, G. H. Lee, J. Hone, T. F. Heinz and J. Shan, *Nat. Mater.*, 2013, **12**, 207–211.

9 J. Chen, M. Badioli, P. Alonso-González, S. Thongrattanasiri, F. Huth, J. Osmond, M. Spasenović, A. Centeno, A. Pesquera, P. Godignon, A. Z. Elorza, N. Camara, F. J. García de Abajo, R. Hillenbrand and F. H. L. Koppens, *Nature*, 2012, **487**, 77–81.

10 K. S. Novoselov, A. K. Geim, S. V. Morozov, D. Jiang, M. I. Katsnelson, I. V. Grigorieva, S. V. Dubonos and A. A. Firsov, *Nature*, 2005, **438**, 197–200.

11 O. Lopez-Sanchez, D. Lembke, M. Kayci, A. Radenovic and A. Kis, *Nat. Nanotechnol.*, 2013, **8**, 497–501.

12 G. Ermolaev, K. Voronin, D. G. Baranov, V. Kravets, G. Tselikov, Y. Stebunov, D. Yakubovsky, S. Novikov, A. Vyshnevyy, A. Mazitov, I. Kruglov, S. Zhukov, R. Romanov, A. M. Markeev, A. Arsenin, K. S. Novoselov, A. N. Grigorenko and V. Volkov, *Nat. Commun.*, 2022, **13**, 2049.

13 Y. V. Stebunov, O. A. Aftenieva, A. V. Arsenin and V. S. Volkov, *ACS Appl. Mater. Interfaces*, 2015, **7**, 21727–21734.

14 C. Liu, X. Chen, H. Luo, B. Li, J. Shi, C. Fan, J. Yang, M. Zeng, Z. Zhou, N. Hu, Y. Su and Z. Yang, *Sens. Actuators B Chem.*, 2021, **347**, 130608.

15 Y. Han, Y. Ma, Y. Liu, S. Xu, X. Chen, M. Zeng, N. Hu, Y. Su, Z. Zhou and Z. Yang, *Appl. Surf. Sci.*, 2019, **493**, 613–619.

16 Y. Han, D. Huang, Y. Ma, G. He, J. Hu, J. Zhang, N. Hu, Y. Su, Z. Zhou, Y. Zhang and Z. Yang, *ACS Appl. Mater. Interfaces*, 2018, **10**, 22640–22649.

17 S. Yu, X. Wu, Y. Wang, X. Guo and L. Tong, *Adv. Mater.*, 2017, **29**, 1606128.

18 W. Du, C. Li, J. Sun, H. Xu, P. Yu, A. Ren, J. Wu and Z. Wang, *Laser Photonics Rev.*, 2020, **14**, 2000271.

19 M. Guizzardi, M. Ghini, A. Villa, L. Rebecchi, Q. Li, G. Mancini, F. Marangi, A. M. Ross, X. Zhu, I. Kriegel and F. Scotognella, *J. Phys. Chem. Lett.*, 2022, **13**, 9903–9909.

20 Y. Shi, X. Liang, B. Yuan, V. Chen, H. Li, F. Hui, Z. Yu, F. Yuan, E. Pop, H.-S. P. Wong and M. Lanza, *Nat. Electron.*, 2018, **1**, 458–465.

21 D. Kireev, K. Sel, B. Ibrahim, N. Kumar, A. Akbari, R. Jafari and D. Akinwande, *Nat. Nanotechnol.*, 2022, **17**, 864–870.

22 G. A. Ermolaev, D. I. Yakubovsky, Y. V. Stebunov, A. V. Arsenin and V. S. Volkov, *J. Vac. Sci. Technol. B*, 2020, **38**, 014002.

23 G. A. Ermolaev, D. V. Grudinin, Y. V. Stebunov, K. V. Voronin,

V. G. Kravets, J. Duan, A. B. Mazitov, G. I. Tselikov, A. Bylinkin, D. I. Yakubovsky, S. M. Novikov, D. G. Baranov, A. Y. Nikitin, I. A. Kruglov, T. Shegai, P. Alonso-González, A. N. Grigorenko, A. V. Arsenin, K. S. Novoselov and V. S. Volkov, *Nat. Commun.*, 2021, **12**, 854.

24 K. F. Mak, C. Lee, J. Hone, J. Shan and T. F. Heinz, *Phys. Rev. Lett.*, 2010, **105**, 136805.

25 J. S. Ponraj, Z.-Q. Xu, S. C. Dhanabalan, H. Mu, Y. Wang, J. Yuan, P. Li, S. Thakur, M. Ashrafi, K. Mccoubrey, Y. Zhang, S. Li, H. Zhang and Q. Bao, *Nanotechnology*, 2016, **27**, 462001.

26 A. B. Evlyukhin, S. M. Novikov, U. Zywietz, R. L. Eriksen, C. Reinhardt, S. I. Bozhevolnyi and B. N. Chichkov, *Nano Lett.*, 2012, **12**, 3749–3755.

27 P. Tonkaev, I. S. Sinev, M. V. Rybin, S. V. Makarov and Y. Kivshar, *Chem. Rev.*, 2022, **122**, 15414–15449.

28 A. A. Popkova, I. M. Antropov, G. I. Tselikov, G. A. Ermolaev, I. Ozerov, R. V. Kirtaev, S. M. Novikov, A. B. Evlyukhin, A. V. Arsenin, V. O. Bessonov, V. S. Volkov and A. A. Fedyanin, *Laser Photonics Rev.*, 2022, **16**, 2100604.

29 K. Koshelev, S. Kruk, E. Melik-Gaykazyan, J.-H. Choi, A. Bogdanov, H.-G. Park and Y. Kivshar, *Science*, 2020, **367**, 288–292.

30 A. V. Prokhorov, S. M. Novikov, M. Y. Gubin, R. V. Kirtaev, A. V. Shesterikov, K. M. Stankevich, D. Yakubovsky, A. V. Arsenin, E. Zhukova, S. S. Zhukov, V. G. Leiman and V. S. Volkov, *ACS Appl. Nano Mater.*, 2022, **5**, 14582–14590.

31 A. V. Prokhorov, A. V. Shesterikov, M. Y. Gubin, V. S. Volkov and A. B. Evlyukhin, *Phys. Rev. B*, 2022, **106**, 035412.

32 H. Lin, Z.-Q. Xu, G. Cao, Y. Zhang, J. Zhou, Z. Wang, Z. Wan, Z. Liu, K. P. Loh, C.-W. Qiu, Q. Bao and B. Jia, *Light Sci. Appl.*, 2020, **9**, 137.

33 A. Krasnok, *Nat. Photon.*, 2020, **14**, 409–410.

34 Y. Li, A. Chernikov, X. Zhang, A. Rigosi, H. M. Hill, A. M. van der Zande, D. A. Chenet, E.-M. Shih, J. Hone and T. F. Heinz, *Phys. Rev. B*, 2014, **90**, 205422.

35 T. D. Green, D. G. Baranov, B. Munkhbat, R. Verre, T. Shegai and M. Käll, *Optica*, 2020, **7**, 680–686.

36 J. B. Khurgin, *ACS Photonics*, 2022, **9**, 743–751.

37 G. Ermolaev, D. Grudinin, K. Voronin, A. Vyshnevyy, A. Arsenin and V. Volkov, *Photonics*, 2022, **9**, 744.

38 H. Ling, R. Li and A. R. Davoyan, *ACS Photonics*, 2021, **8**, 721–730.

39 B. Munkhbat, D. G. Baranov, M. Stührenberg, M. Wersäll, A. Bisht and T. Shegai, *ACS Photonics*, 2019, **6**, 139–147.

40 R. Verre, D. G. Baranov, B. Munkhbat, J. Cuadra, M. Käll and T. Shegai, *Nat. Nanotechnol.*, 2019, **14**, 679–683.

41 P. G. Zotev, Y. Wang, L. Sortino, T. S. Millard, N. Mullin, D. Conteduca, M. Shagar, A. Genco, J. K. Hobbs, T. F. Krauss and A. I. Tartakovskii, *ACS Nano*, 2022, **16**, 6493–6505.

42 S. Busschaert, R. Reimann, M. Cavigelli, R. Khelifa, A. Jain and L. Novotny, *ACS Photonics*, 2020, **7**, 2482–2488.

43 F. Hu, Y. Luan, J. Speltz, D. Zhong, C. H. Liu, J. Yan, D. G. Mandrus, X. Xu and Z. Fei, *Phys. Rev. B*, 2019, **100**, 121301(R).

44 A. A. Ushkov, G. A. Ermolaev, A. A. Vyshnevyy, D. G. Baranov, A. V. Arsenin and V. S. Volkov, *Phys. Rev. B*, 2022, **106**, 195302.

45 G. I. Tselikov, G. A. Ermolaev, A. A. Popov, G. V. Tikhonowski, D. A. Panova, A. S. Taradin, A. A. Vyshnevyy, A. V. Syuy, S. M. Klimentov, S. M. Novikov, A. B. Evlyukhin, A. V. Kabashin, A. V. Arsenin, K. S. Novoselov and V. S. Volkov, *Proc. Natl. Acad. Sci. U.S.A.*, 2022, **119**, e2208830119.

46 B. Munkhbat, A. B. Yankovich, D. G. Baranov, R. Verre, E. Olsson and T. O. Shegai, *Nat. Commun.*, 2020, **11**, 4604.

47 R. Mupparapu, M. Steinert, A. George, Z. Tang, A. Turchanin, T. Pertsch and I. Staude, *Adv. Mater. Interf.*, 2020, **7**, 2000858.

48 A. Castellanos-Gomez, M. Barkelid, A. M. Goossens, V. E. Calado, H. S. J. van der Zant and G. A. Steele, *Nano Lett.*, 2012, **12**, 3187–3192.

49 A. H. Atabaki, S. Moazeni, F. Pavanello, H. Gevorgyan, J. Notaros, L. Alloatti, M. T. Wade, C. Sun, S. A. Kruger, H. Meng, K. A. Qubaisi, I. Wang, B. Zhang, A. Khilo, C. V. Baiocco, M. A. Popović, V. M. Stojanović and R. J. Ram, *Nature*, 2018, **556**, 349–354.

50 M. Li, S. Biswas, C. U. Hail and H. A. Atwater, *Nano Lett.*, 2021, **21**, 7602–7608.

51 A. Raja, L. Waldecker, J. Zipfel, Y. Cho, S. Brem, J. D. Ziegler, M. Kulig, T. Taniguchi, K. Watanabe, E. Malic, T. F. Heinz, T. C. Berkelbach and A. Chernikov, *Nat. Nanotechnol.*, 2019, **14**, 832–837.

52 A. V. Kabashin and M. Meunier, *J. Appl. Phys.*, 2003, **94**, 7941.

53 A. A. Popov, Z. Swiatkowska-Warkocka, M. Marszalek, G. Tselikov, I. V. Zelepukin, A. Al-Kattan, S. M. Deyev, S. M. Klimentov, T. E. Itina and A. V. Kabashin, *Nanomaterials*, 2022, **12**, 649.

54 S. Besner, A. Kabashin and M. Meunier, *Appl. Phys. A*, 2007, **88**, 269–272.

55 P. Blandin, K. A. Maximova, M. B. Gongalsky, J. F. Sanchez-Royo, V. S. Chirvony, M. Sentis, V. Y. Timoshenko and A. V. Kabashin, *J. Mater. Chem. B*, 2013, **1**, 2489–2495.

56 A. A. Popov, G. Tselikov, N. Dumas, C. Berard, K. Metwally, N. Jones, A. Al-Kattan, B. Larrat, D. Braguer, S. Mensah, A. Da Silva, M.-A. Estève and A. V. Kabashin, *Sci. Rep.*, 2019, **9**, 1194.

57 F. Ye, D. Chang, A. Ayub, K. Ibrahim, A. Shahin, R. Karimi, S. Wettig, J. Sanderson and K. P. Musselman, *Chem. Mater.*, 2021, **33**, 4510–4521.

58 H. Xu, L. Zhang, A. Wang, J. Hou and X. Guo, *Nanomaterials*, 2021, **11**, 3192.

59 G. Eda, G. Fanchini and M. Chhowalla, *Nat. Nanotechnol.*, 2008, **3**, 270–274.

60 S. J. Sandoval, D. Yang, R. F. Frindt and J. C. Irwin, *Phys. Rev. B*, 1991, **44**, 3955.

61 Y. Sun, K. Liu, X. Hong, M. Chen, J. Kim, S. Shi, J. Wu, A. Zettl and F. Wang, *Nano Lett.*, 2014, **14**, 5329–5334.

62 A. B. Evlyukhin, T. Fischer, C. Reinhardt and B. N. Chichkov, *Phys. Rev. B*, 2016, **94**, 205434.

63 A. B. Evlyukhin and B. N. Chichkov, *Phys. Rev. B*, 2019, **100**, 125415.
64 X. Li and H. Zhu, *J. Materiomics*, 2015, **1**, 33–44.
65 Y. Zhao and G. Ouyang, *Sci. Rep.*, 2019, **9**, 17381.
66 M. Dieterle, G. Weinberg and G. Mestl, *Phys. Chem. Chem. Phys.*, 2002, **4**, 812–821.
67 S. Balendhran, J. Deng, J. Z. Ou, S. Walia, J. Scott, J. Tang, K. L. Wang, M. R. Field, S. Russo, S. Zhuiykov, M. S. Strano, N. Medhekar, S. Sriram, M. Bhaskaran and K. Kalantar-zadeh, *Adv. Mater.*, 2013, **25**, 109–114.
68 A. Arash, S. A. Tawfik, M. J. S. Spencer, S. K. Jain, S. Arash, A. Mazumder, E. Mayes, F. Rahman, M. Singh, V. Bansal, S. Sriram, S. Walia, M. Bhaskaran and S. Balendhran, *ACS Appl. Mater. Interfaces*, 2020, **12**, 16997–17003.
69 J. Ryou, Y.-S. Kim, S. KC and K. Cho, *Sci. Rep.*, 2016, **6**, 29184.
70 Y. Zhu, Y. Yao, Z. Luo, C. Pan, J. Yang, Y. Fang, H. Deng, C. Liu, Q. Tan, F. Liu and Y. Guo, *Molecules*, 2020, **25**, 18.
71 S. Meng, Y. Zhang, H. Wang, L. Wang, T. Kong, H. Zhang and S. Meng, *Biomaterials*, 2021, **269**, 120471.
72 L. Wang, D. Xu, L. Jiang, J. Gao, Z. Tang, Y. Xu, X. Chen and H. Zhang, *Adv. Funct. Mater.*, 2021, **31**, 2004408.
73 U. Zywietz, A. B. Evlyukhin, C. Reinhardt and B. N. Chichkov, *Nat. Commun.*, 2014, **5**, 3402.
74 A. B. Evlyukhin, M. A. Poleva, A. V. Prokhorov, K. V. Baryshnikova, A. E. Miroshnichenko and B. N. Chichkov, *Laser Photonics Rev.*, 2021, **15**, 2100206.

Journal of Materials Chemistry C

CORRECTION

Cite this: *J. Mater. Chem. C*, 2023, **11**, 5890

Correction: Tunable optical properties of transition metal dichalcogenide nanoparticles synthesized by femtosecond laser ablation and fragmentation

Anton S. Chernikov,[a] Gleb I. Tselikov,[bc] Mikhail Yu. Gubin,*[ba] Alexander V. Shesterikov,[ba] Kirill S. Khorkov,[a] Alexander V. Syuy,[bc] Georgy A. Ermolaev,[bc] Ivan S. Kazantsev,[bc] Roman I. Romanov,[d] Andrey M. Markeev,[b] Anton A. Popov,[d] Gleb V. Tikhonowski,[cd] Olesya O. Kapitanova,[be] Dmitry A. Kochuev,[a] Andrey Yu. Leksin,[a] Daniil I. Tselikov,[d] Aleksey V. Arsenin,[bcf] Andrei V. Kabashin,[g] Valentyn S. Volkov[c] and Alexei V. Prokhorov[ba]

DOI: 10.1039/d3tc90084c

rsc.li/materials-c

Correction for 'Tunable optical properties of transition metal dichalcogenide nanoparticles synthesized by femtosecond laser ablation and fragmentation' by Anton S. Chernikov *et al.*, *J. Mater. Chem. C*, 2023, **11**, 3493–3503, https://doi.org/10.1039/D2TC05235K.

The authors regret that the affiliation of Andrei V. Kabashin was incorrect in the published article. The correct affiliation of Andrei V. Kabashin is "CNRS, LP3, Aix-Marseille Université, Marseille 13288, France", and not "National Research Nuclear University MEPhI, Moscow 115409, Russia", as was given in the published article. The correct list of authors and affiliations is given above.

The Royal Society of Chemistry apologises for these errors and any consequent inconvenience to authors and readers.

[a] *Department of Physics and Applied Mathematics, Vladimir State University named after A. G. and N. G. Stoletovs (VlSU), Vladimir 600000, Russia*
[b] *Center for Photonics and 2D Materials, Moscow Institute of Physics and Technology, Dolgoprudny 141701, Russia. E-mail: myugubin@gmail.com*
[c] *Emerging Technologies Research Center, XPANCEO, Dubai Investment Park First, Dubai, United Arab Emirates*
[d] *National Research Nuclear University MEPhI, Moscow 115409, Russia*
[e] *Faculty of Chemistry, Lomonosov Moscow State University, Moscow 119991, Russia*
[f] *Laboratory of Advanced Functional Materials, Yerevan State University, Yerevan 0025, Armenia*
[g] *CNRS, LP3, Aix-Marseille Université, Marseille 13288, France*